CSCE Annual Conference

Growing with youth – Croître avec les jeunes

Laval (Greater Montreal)

June 12 - 15, 2019

PUNCHING BEHAVIOR OF GFRP-RC SLAB-COLUMN CONNECTION UNDER REVERSED LATERAL CYCLIC LOADING

Mohamed Eladawy[1, 2], Mohamed Hassan[1, 3], and Brahim Benmokrane[1, 4]
[1] Department of Civil and Building Engineering, University of Sherbrooke - Sherbrooke, QC, Canada.
[2] Mohamed.Eladawy@Ushearbrooke.ca
[3] Mohamed.Hassan@USherbrooke.ca
[4] Brahim.Benmokrane@USherbrooke.ca

Abstract: This study investigates the seismic behavior of interior flat slab-column connection reinforced with glass fiber-reinforced polymer (GFRP) bars. Total of three full-scale slab-column connections were constructed and tested under combined gravity and quasi-static revered lateral cyclic loading until failure. The slabs measured 2500 mm × 2500 mm × 200 mm and supported by a square column of 300 mm × 300 mm extended above and below the slab thickness of a distance 700 mm. This paper outlines the effect of using GFRP bars as reinforcement on the seismic behavior of the tested connection. The seismic performance of the slab-column connections is evaluated on the basis of the experimentally recorded moment–lateral drift hysteretic relationships and mode of failure. The test results revealed that GFRP slab-column connection exhibited adequate strength against punching failure. The GFRP specimen achieved lateral inter-story drift capacities over 1.50 % satisfying the limitations in the CSA A23.3 and ACI 421.3R. This paper provides a step forward for engineers and researchers to better understanding the seismic behavior of GFRP-reinforced two-way concrete slabs under cyclic lateral loading. However, more experimental tests are needed to establish design provisions and recommendations for designing FRP-reinforced two-way in seismic zones.

1 INTRODUCTION

Flat plate structures are common in reinforced concrete structures due to their functional and economic advantages. This system, however, can experience a brittle punching failure at the slab-column connection due to high shearing forces and unbalanced moments between the slabs and columns. The shear transfer usually comes from the gravity load while the unbalanced moments may come from different loading between the adjacent span, or lateral loading, such as strong wind or earthquake. In moderate and high seismic zones, flat plate structures are coupled with either a moment-resisting frame or shear wall lateral force-resisting system. The ductility of these systems is generally limited by the deformation capacity of the slab-column connections. Therefore, slab-column connections must possess adequate strength against punching failure during and after earthquake occurrence and adequate ductility to undergo inelastic deformations without failure, that is, the ability to withstanding at least 1.5% inter-story drift ratio. Inter-story drift ratio is the difference of lateral defection between two successive floors divided by the floor height. The 1.5% is a frequently recommended minimum inter-story drift ratio that a multistory structure should

withstand in a seismic zone without failure (Moehle et al. 1988, Megally et al. 2000 and Robertson et al. 2006).

Applications of glass fiber-reinforced polymer (GFRP) composites as reinforcement for concrete structures have been growing rapidly in recent years. The corrosion resistance of GFRP reinforcement is a significant benefit for structures in highly corrosive environments such as parking garages treated with de-icing salts. Concrete slabs in parking garages deteriorate faster than any other structural components because of the direct exposure to the environment and de-icing chemicals. Using GFRP bars in reinforced concrete reinforced concrete slabs can extend the service life, reduce maintenance costs, and improve the life-cycle cost efficiency (Benmokrane et al. 2012 and Ahmed et al. 2017). GFRP reinforcement has a high tensile strength, significant elongation, and exhibits linear stress-strain behavior to failure. Due to the differences in the GFRP materials behavior versus steel, unique guidance on the engineering and construction of concrete structures reinforced with GFRP bars is necessary. Although there is a substantial amount of information on the flexural and shear performance of FRP-reinforced concrete elements, behavior under combined vertical shear forces and static or cyclic lateral loading for FRP-reinforced two-way flat plate/slab are still lacking (ACI 440.1R 2015).

The previous tests conducted on two-way FRP-reinforced concrete slabs focused on the punching-shear behavior under monotonic concentric loading only (El-Ghandour et al. 2003; Ospina et al. 2003; and Hassan et al. 2013). Few studies have been investigated the punching-shear behavior of interior FRP slab-column connections subjected to shear load and static unbalanced moment (Gouda et al. 2015; and Hussein et al. 201]. The results revealed that, the basic punching-shear behaviour of the FRP- reinforced concrete slab-column connections were comparable to steel- reinforced concrete connections. In addition, the column aspect ratio, slab thickness, shear reinforcement and using high-strength concrete had significant effect on the punching shear capacity and the deformation capacity of the slabs. This study aimed to understanding and assessing the punching-shear behavior of two way GFRP specimen under quasi-static reversed cyclic loading to simulate seismic loading. Based on the laboratory testing results, the punching-shear performances are evaluated in terms of modes of failure, cracking patterns, hysteretic response, reinforcement and concrete strains.

2 EXPERIMENTAL PROGRAM

2.1 Material Properties

Two sizes of grade III sand-coated GFRP reinforcing bars (No. 15 and No. 20, as classified in CSA S807 (2015), were used as flexural reinforcement in the GFRP-reinforced specimens. The GFRP bars were manufactured by combining the pultrusion process with an in-line sand-coating process for the bar surface. This sand coating was designed to improve bonding between the GFRP bars and surrounding concrete. The tensile properties of the GFRP bars were determined according to ASTM D7205 (2011). Deformed 25M steel bars were used to reinforce the column. Table 1 summarizes the mechanical properties of the GFRP and steel reinforcement. The slab specimen was cast using a ready-mixed, normal-weight concrete with 5% to 8% entrained air. The bottom and top columns were cast simultaneously with the slab on the same day. The concrete compressive (f_c') and tensile strengths (f_t) for specimen was determined on the day of testing from nine concrete cylinders measuring 100×200 mm. The cylinders were cast simultaneously with the slab. Table 2 provides the concrete properties of the specimen.

Table 1: Mechanical properties of the GFRP reinforcing bars

RFT Type	Grade	Bar size	Area (mm^2)	Elastic Tensile Modulus. E_f, (GPa)	Ultimate Tensile Strength, (MPa)	Ultimate Tensile Elongation (%)
GFRP	III	No.15	199	62.6±2.50	1239±51	1.89±0.10
		No.20	285	64.9±0.60	1334±85	2.07±0.13
Steel	44W	25M	490	200	620	0.24

2.2 Specimen Details

Figure 1 shows the typical geometry of the test specimen and reinforcement details. The test specimen was designed in accordance with CSA S806 (2012). The specimen was measured 2500×2500 mm with a thickness of 200 mm. A column measuring 300 mm×300 mm measuring extended 700 mm at its centre above and below the slab surfaces. These dimensions were consistent with an extensive research project conducted at the University of Sherbrooke to evaluate the punching-shear performance of GFRP-RC slab–column connections (Dulude et al. 2013 and Hassan et al. 2013).

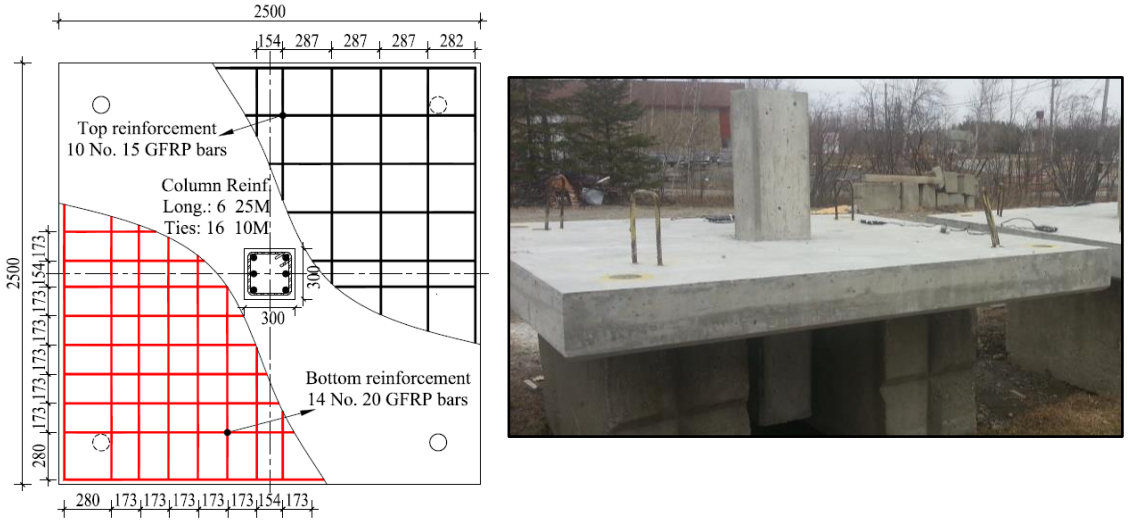

Figure 1: Dimensions and reinforcement details of the test specimen

The specimen had a typical bottom- and top-reinforcement configuration in each orthogonal direction, as shown in Figure 1. The specimen was designed to have a flexural-reinforcement ratio such that punching-shear failure would be expected to occur prior to flexural failure. The bottom flexural-reinforcement placed symmetrically in each orthogonal direction and consisted of 14 No. 20 bars. The top flexural-reinforcement placed symmetrically in each orthogonal direction and consisted of 10 No. 15 bars. The reinforcing ratio on the compression side was half that of the tension reinforcement. Two bars ran through the column core on the compression side to satisfy the requirements for structural-integrity reinforcement in CSA A23.3 (2014). The clear concrete cover in the direction of the lateral cycling loads was 30 mm. The average effective depth of the slabs d was 151 mm.

The column was heavily reinforced with steel bars (reinforcement ratio of 3.0%) to make the column strong enough to transfer shear force and cyclic moments to the slab and to avoid column failure during testing. The column was reinforced with six longitudinal deformed 25M steel bars. In addition, closed deformed 10M steel ties were used spaced at 100 mm.

2.3 Instrumentation

Each specimen had a group of displacement transducers to monitor the vertical displacement and column lateral displacement (Figure 2). On the top slab face, nine pots were installed vertically along two perpendicular directions at 100, 300, and 600 mm from the column face. One pot was attached horizontally to both ends of the column to measure lateral-drift. Two horizontal pots were also installed on the centerline of the slab thickness and the lower supporting frame to monitor any movement in the lateral-loading direction. The flexural-crack widths were measured with two LVDTs on the slab tension face. The LVDTs were installed at the locations of the first flexural cracks in each direction. Two instrumented bars were installed in both orthogonal directions on the bottom flexural-reinforcement. Five electrical strain gauges were attached to each bar at 0, 75, 225, 450, and 750 mm from the column face. In addition, one strain gauge was attached to the top reinforcing bar (compression side) at the column face in both orthogonal directions. Six concrete electrical strain gauges were glued to the compression face of the slab to record concrete strains: four at the comers of the column in the direction of the lateral loads and two in the transverse direction. The strain gauges, pots, and LVDTs were connected to a data-acquisition system to record all values.

Figure 2: Position of internal and external instrumentations.

2.4 Test Setup and Test Procedure

Figure 3 shows the setup used to test all specimens. The setup had two main supporting frames. The supporting frame, which had two parts, was intended to carry the applied vertical load. The first part-the lower supporting bed consisted of steel bottom reaction box-beams tied to four supporting steel box-columns. It was also laterally stiffened with back-to-back steel angles. The lower steel bed was prestressed directly on the laboratory floor with four vertical Dywidag bars. The second part consisted of the steel upper reaction box-beams. It served to restrain the specimen from overturning due to lateral loads. Thick neoprene pads were placed between the specimen and the lower and upper reaction beams. The upper steel box-beams with the specimen and the lower supporting frame were fixed to the floor using four steel nuts and plates attached to the vertical Dywidag bars.

The second supporting frame consisted of two lateral steel frames. The frames were firmly fixed to the laboratory floor with four vertical Dywidag bars. To restrain any possible frame lateral sway, two steel box -beams were installed between two lateral steel frames and the lower supporting bed. A 1000 kN capacity hydraulic Enerpac jack was attached to a stiff steel reaction I-beam to apply the gravity load at the top of the column. To maintain the vertical load on the column during its lateral reversed movements, a rectangular steel plate with a crosshead was connected to the Enerpac jack. On the other hand, to reduce the friction between the column and the head of the Enerpac jack, a steel plate with steel rollers was fabricated and installed on the top of the upper column, as shown in Figure 3. Two 250 kN capacity horizontal hydraulic actuators were attached to the lateral frames and connected to the column ends to apply cyclic lateral-drift load.

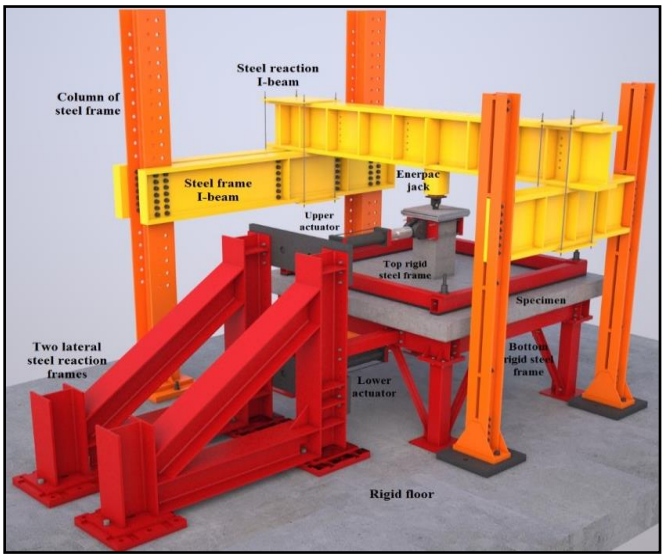

Figure 3: Experimental setup.

At the beginning, a concentric load was applied to the top of the upper column in a load-control mode and at a loading rate of 20 kN/min. The desired load was approximately 140 kN. This value represented the dead load plus 30% of the live load on a typical floor-system prototype. The horizontal actuators were then activated to apply the lateral reversed loads on the column ends. The actuators operated in displacement-control mode. The actuators pushed and pulled the column ends simultaneously at the same rate according to a planned cyclic-loading pattern but in different directions (see Figure 4). The positive drift in the routine corresponds to the actuator pushing the column, whereas the negative drift corresponds to the actuator pulling the column. Each increment represents an approximate increase in the lateral inter-story drift ratio of 0.25%. Each cycle at a new drift level was performed twice to evaluate the loss of specimen strength and stiffness during the repeated cycles.

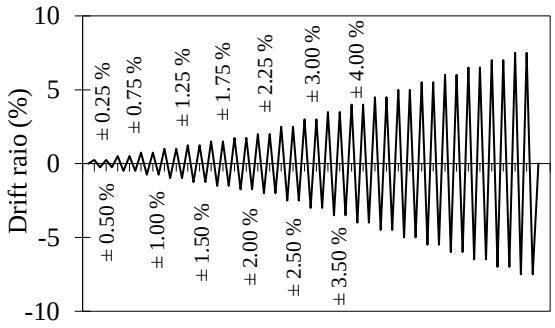

Figure 4: Lateral displacement routine.

3 TEST RESULTS AND OBSERVATIONS

3.1 Cracking Behavior

Figure 5 shows the cracking pattern development for the specimen under gravity and reversed lateral cyclic loading. In general, four kinds of typical cracks were observed on the slab tension side. After the application of the gravity load, initial radial flexural cracks originated from the slab–column interface and propagated towards the supports. The cracks began to appear at gravity loads of 135 kN. With the application of the initial displacement cycles, diagonal cracks were radiated from the column corner to the slab boundaries and additional radial cracks were formed. At drift ratios ranged between 0.50 to 0.75%, inclined torsional

cracks at column sides were initiated and originated from 35 to 45 degrees to the lateral loading direction. After completion of 0.75% drift cycles, tangential cracks were generated around the column and crossed over the radial and diagonal cracks. As of 1.00% to 1.25% lateral drifts, the number of such cracks and their widths in the column vicinity were significantly increased. However, these cracks were generally stabilized with only few new cracks occurred at 2.00% drift. At ultimate lateral load, a major tangential crack was intercepted by the flexural cracks in approximately perpendicular manner forming the punching cone in one side of the slab at ultimate drifts of 2.25%. After completion of the second repeated cycles, a complete punching failure surface was totally formed as shown in Figure 5.

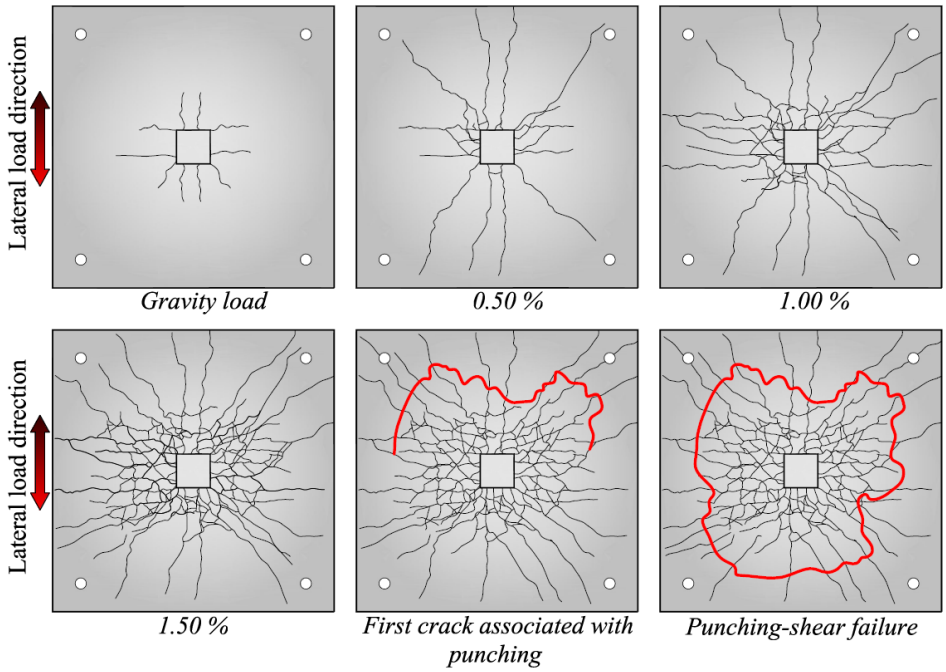

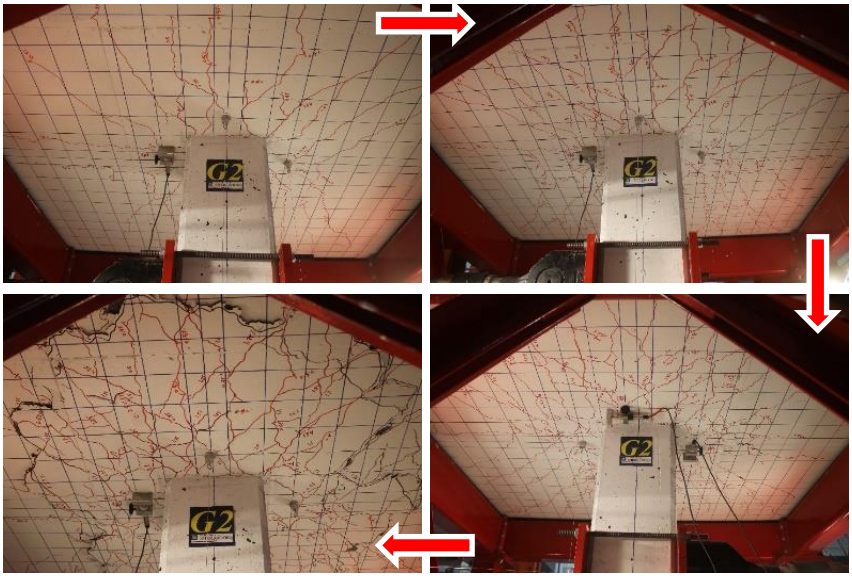

Figure 5: Cracking pattern development.

The specimen failed suddenly in a brittle punching shear failure. The maximum radial crack widths were 1.15 mm corresponding to ultimate drift of 2.25%. The average distance between the column face and the perimeter of the failure cone along the lateral-load direction was 4.0*d* compared to 4.8*d* along the transverse direction, respectively. Figure 6 shows sawn sections for the specimen through a line parallel to direction of lateral loading and adjacent to the column. The punching failure was characterized by a single diagonal shear crack started from the column face to the slab tension side with different inclination angles as seen in Figure 6. The average angle of the inclined shear cracks was about 24º with respect to the slab tension side. Steep shear cracks due to load reversals indicate severe concrete degradation that limits deformation capacity of the connection (Drakatos et al. 2016).

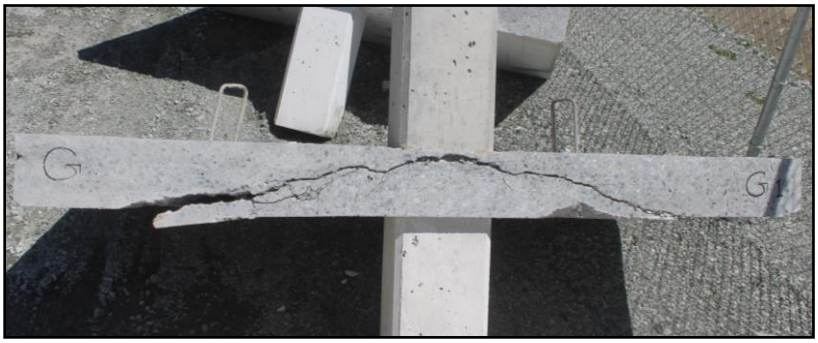

Figure 6: Saw-cut along the load direction.

3.2 Moment–Lateral Drift Hysteretic Response

Figure 7 provides the unbalanced moment versus lateral-drift-ratio relationship for the specimen. The unbalanced moments were calculated by multiplying the two lateral forces, applied to each column by the distance from the application point to the center of the slab: 675 mm. The lateral drift ratio was calculated as the ratio of the sum of measured displacements at the column ends to the distance between the two loading rams. Table 2 provides the peak lateral load, maximum unbalanced moment, and corresponding lateral-drift ratio in each direction. In general, the test specimen demonstrated stable hysteresis response until failure occurred at the end. The specimen displayed also good ability to withstand inter-story drift up to the level of 1.5%, minimum drift capacity, without punching failure.

Table2: Test results

Specimen	f'_c MPa	Gravity-Load V_g (kN)	Peak Lateral Load KN		Max. Unbalanced Moment KN.m		Drift Ratio (%)	
			H_+	H_-	*M*+	*M*-	*δ*+	*δ*-
G	52	140	136.6	136.7	179.8	180.9	2.25	-2.25

(+) refers to the positive direction and (-) to the negative direction Compression and splitting testing on 100×200 mm concrete cylinders.

As seen in Figure 7 a sudden drop in the overall hysteretic loops immediately after punching of the connection indicated the rapid loss of stiffness of the connection. The specimen failed in punching after the peak unbalanced moment transfer of 180.9 kN.m at 2.25% drift ratio and was indicated a sudden load drop of approximately 78% of its capacity in the subsequent loading, respectively. A slight strength reduction was observed ranged from 2 to 4% at drift ratio between 0.25 to 1.00% after the application of the second repeated cycle. However, this reduction was increased up to 6% after 1.25% drift ratio until failure.

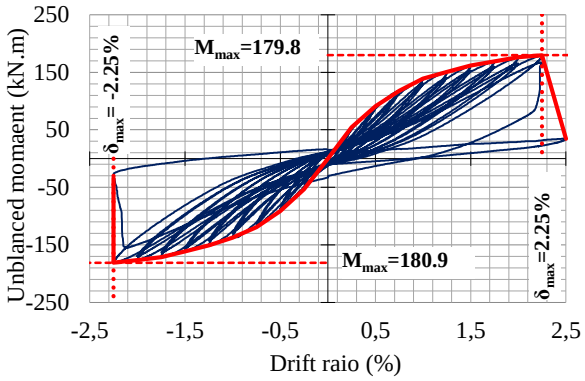

Figure 7: Unbalanced moment versus lateral drift ratio.

3.3 Assessment of CSA-S806 Punching-Shear Equations

The predicated ultimate unbalanced moment capacity (M_{CSA}) was calculated using the eccentric shear-stress model with a fraction (γ_v), and resisted by the shear at the perimeter of d/2 from the column face using Eqns. (1). The punching-shear strength provided by CSA-S806-2012 is calculated as the smallest of Eqns. (2) to (4). The critical perimeter nearest a column equal to 0.5 times the effective depth of 0.5*d* was taken, where (λ) is the concrete density factor; (φ_c) is the concrete resistance factor; (βc) is the ratio of the long side to the short side of the column (αs=4); and (f_c') shall not exceed 60 MPa. The CSA S806 (2012) equations yielded reasonable and conservative prediction with average $M_{exp}/M_{pred.}$ of 1.30

[1] $$M_n = \frac{J_x}{i_v e}\left[v_{max} - \frac{V_n}{b_o d_v}\right]$$

[2] $$V_c = 0.056\lambda f_c \left(E_f\ \rho_f\ f_c'\right)^{1/3} b_{0.5d} d$$

[3] $$V_c = 0.147\lambda f_c \left(0.19 + \frac{\alpha_c d}{\beta_c}\right)\left(E_f\ \rho_f\ f_c'\right)^{1/3} b_{0.5d} d$$

[4] $$V_c = 0.028\lambda f_c \left(1 + \frac{2}{\beta_c}\right)\left(E_f\ \rho_f\ f_c'\right)^{1/3} b_{0.5d} d$$

4 Conclusions

1. The GFRP-reinforced specimen experienced a typical sudden and brittle punching-shear failure without much warning. The punching-shear failure was evidenced by a sudden drop in the applied gravity and lateral loads.
2. The GFRP-reinforced specimen showed stable hysteresis response until failure and the punching failure was governed by the strength of the connection.
3. The GFRP-reinforced specimen displayed adequate ability to withstand inter-story drift up to the level of 1.5%, minimum drift capacity, without punching failure.
4. GFRP reinforcing bars could be used effectively as reinforcement in slab–column connections subjected to gravity and reversed lateral cyclic loads.
5. The predicted ultimate unbalanced moment capacity provided by CSA S806 (2012) equations were reasonable and conservative with average M_{exp}/M_{pred} of 1.30.

ACKNOWLEDGEMENTS

The authors wish to express their gratitude and sincere appreciation to the Natural Science and Engineering Research Council of Canada (NSERC), the NSERC Research Chair in Innovative FRP Reinforcement for Concrete Structures, the Tier-1 Canada Research Chair in Advanced Composite Materials for Civil structures, the Fonds Québécois de la Recherche sur la Nature et les Technologies (FQRNT), the Canadian Foundation for Innovation (FCI), and the exceptional efforts of the technical staff of the CFI structural laboratory in the Department of Civil Engineering at the University of Sherbrooke.

References

American Concrete Institute (ACI Committee 421), 2010. *Guide to Seismic Design of Punching Shear Reinforcement in Flat Plates (ACI 421.2R-2010)*, ACI, Farmington Hills, Mich.

American Concrete Institute (ACI Committee 440) 2004. *Guide Test Methods for Fiber-Reinforced Polymers (FRPs) for Reinforcing or Strengthening Concrete Structures (ACI 440.3R-04)*. ACI, Farmington Hills, MI, 40 pp.

American Concrete Institute (ACI Committee 440), 2015. *Guide for the Design and Construction of Structural Concrete Reinforced with Fiber-Reinforced Polymer (FRP) Bars (ACI 440.1R-2015)*, Farmington Hills, MI.

American Society for Testing and Materials (ASTM D7205M), 2011. *Standard test method for tensile properties of fiber reinforced polymer matrix composite bars*. Conshohocken, USA. p.12.

Benmokrane, B., Ahmed, E., Dulude, C., and Boucher, E. 2012. Design, Construction, and Monitoring of the First Worldwide Two-Way Flat Slab Parking Garage Reinforced with GFRP Bars. Proceedings of the *6th International Conference on FRP Composites in Civil Engineering*, Rome, Italy, June 13-15, 8 p.

Canadian Standards Association (CSA), 2012. *Design and Construction of Building Structures with Fiber Reinforced Polymers (CAN/CSA S806–12)*, Rexdale, Ontario, Canada, 198 p.

Canadian Standards Association (CSA), 2014. *Canadian highway bridge design code (CAN/CSA S6-14),* Rexdale, Ontario, Canada, 798 p.

Canadian Standards Association (CSA), 2014. *Design of concrete structures for buildings (CSA-A23.3 M-14),* Rexdale, Ontario, Canada, 240 p.

Canadian Standards Association (CSA), 2015. *Specification for Fiber-Reinforced Polymers (CAN/CSA S807–15)*, Rexdale, Ontario, Canada, 27 p.

Dulude, C., Hassan, M., Ahmed, E.A., and Benmokrane, B., 2013. Punching Shear Behaviour of Two-Way Flat Concrete Slabs Reinforced with GFRP Bars. *ACI Structural Journal*, 110(5): 723–734.

El-Ghandour, A.W.; Pilakoutas, K.; and Waldron P., 2003. Punching Shear Behavior of Fiber Reinforced Polymers Reinforced Concrete Flat Slabs: Experimental Study. *ASCE Journal of Composites for Construction*, 7(3): 258–265.

Gouda, A., and El-Salakawy, E., 2015. Punching Shear Strength of GFRP-RC Interior Slab-Column Connections Subjected to Moment Transfer. *American Society of Civil Engineers,* DOI: 10.1061/ (ASCE) CC.1943-5614.0000597.

Hassan, M., Ahmed, E. A., and Benmokrane, B., 2013. Punch¬ing-Shear Strength of GFRP-Reinforced Concrete Flat Slabs. *Canadian Journal of Civil Engineering*, V. 40, No. 10, Apr., pp. 951-960.

Hussein, A., and El-Salakawy, E., 2018. Punching Shear Behavior of Glass Fiber-Reinforced Polymer-Reinforced Concrete Slab-Column Interior Connections. *ACI Structural Journal,* V. 115, No. 4, July 2018. MS No. S-2017-264.R1, doi: 10.14359/51702134.

Megally, S., and Ghali, A., 1998. *Punching Shear Resistance of Concrete Slabs to Gravity and Earthquake Forces.* PhD thesis, Department of Civil Engineering, Calgary University, Alberta, Canada, 504 p.

Osman M., Marzouk H., and Helmy S., 2000. Behavior of High-Strength Lightweight Concrete Slabs under Punching Loads. *ACI Structural Journal,* V. 97, No. 3. May-June 2000, pp. 99-097.

Ospina, C.E.; Alexander, S.D. B.; and Roger Cheng, J.J., 2003. Punching of Two-Way Concrete Slabs with Fiber-Reinforced Polymer Reinforcing Bars or Grids. *ACI Structural Journal,* 100(5): 589–598.

Pan, A., and Moehle, J.P., 1988. Lateral Displacement Ductility of Reinforced Concrete Flat Plates. *ACI Structural Journal,* V. 86, No. 3, May-June 1989, pp. 250-258.

Robertson I. and Johnson G., 2006. Cyclic Lateral Loading of Non-ductile Slab-Column Connections. *ACI Structural Journal,* V. 103, No. 3, May-June 2006. pp. 04-194.

Robertson NI., and Durrani AJ., 1992. Gravity Load Effect on Seismic Behavior of Interior Slab-Column Connection. *ACI Structural Journal*, V. 98, No. 1, Jan-Feb 1992. pp. 89-S5.